Applied Catalysis B: Environmental 90 (2009) 470–477

Contents lists available at ScienceDirect

Applied Catalysis B: Environmental

journal homepage: www.elsevier.com/locate/apcatb

Alumina supported Pt(1%)/$Ce_{0.6}Zr_{0.4}O_2$ monolith: Remarkable stabilization of ceria–zirconia solution towards $CeAlO_3$ formation operated by Pt under redox conditions

L.F. Liotta [a,*], A. Longo [a], G. Pantaleo [a], G. Di Carlo [b], A. Martorana [b], S. Cimino [c], G. Russo [d], G. Deganello [a,b]

[a] Istituto per lo Studio dei Materiali Nanostrutturati (ISMN)-CNR, via Ugo La Malfa 153, 90146 Palermo, Italy
[b] Dipartimento di Chimica Inorganica ed Analitica "Stanislao Cannizzaro", Università di Palermo, Viale delle Scienze – Parco d'Orleans II, 90128 Palermo, Italy
[c] Istituto di Ricerche sulla Combustione (IRC) – CNR, P.le Tecchio 80, 80125 Napoli, Italy
[d] Dipartimento di Ingegneria Chimica-Università degli Studi di Napoli "Federico II", P.le Tecchio 80, 80125 Napoli, Italy

ARTICLE INFO

Article history:
Received 29 January 2009
Received in revised form 26 March 2009
Accepted 4 April 2009
Available online 11 April 2009

Keywords:
$Pt/Ce_{0.6}Zr_{0.4}O_2$/alumina
cordierite monolith
Rietveld refinement
$CeAlO_3$ formation
TEM/SEM investigations
CO and C_3H_6 oxidation
NO SCR

ABSTRACT

A structured Pt(1 wt%)/ceria–zirconia/alumina catalyst and the metal-free ceria–zirconia/alumina were prepared, by dip-coating, over a cordierite monolithic support. XRD analyses and Rietveld refinements of the structural data demonstrate that in the Pt supported catalysts ceria–zirconia is present as a $Ce_{0.6}Zr_{0.4}O_2$ homogeneous solid solution and that the deposition over the cordierite doesn't produce any structural modification. Moreover no Pt sintering occurs.

By comparing the XRD patterns recorded on Pt/ceria–zirconia/alumina and ceria–zirconia/alumina after three redox cycles, it results that Pt, favouring the structural reorganization of the ceria–zirconia into one cubic solid solution, prevents any $CeAlO_3$ formation. On the contrary, such phase due to the interaction between Ce^{3+} and the alumina present in the washcoat is detected when redox cycles are carried out on the ceria–zirconia metal free.

Transmission electron microscopy (TEM) investigations of the redox cycled Pt/ceria–zirconia/alumina catalyst detected ceria–zirconia grains with diameter between 10 and 35 nm along with highly dispersed Pt particles (2–3 nm) strongly interacting with ceria.

Scanning electron microscopy (SEM) and EDX analyses, recorded on the redox cycled Pt/ceria–zirconia/alumina washcoated monolith evidence a homogeneous distribution of the active components through the channels even after redox aging.

Reduction behaviour and CO oxidation activity are in good agreement with the structural modification of the solid solution induced by the redox cycles and reflect the positive effect of Pt/ceria interaction on the catalytic performances.

The effect of redox aging on the NO reduction by C_3H_6, in lean conditions, was investigated over the Pt/ceria–zirconia/alumina monolith. The catalyst shows at low temperature (290 °C) good NO removal activity and appreciable selectivity to N_2.

1. Introduction

Modern three-way catalysts (TWCs) technology for the 2000s uses monolithic washcoated catalysts with precious metals (Pt, Pd, Rh) supported on oxygen storage components, such as ceria–zirconia mixed oxides [1]. Ceria, stabilized in solid solution with zirconia for high-temperature operations, can easily release or uptake oxygen in the reaction environment, due to the low redox potential of the Ce^{4+}–Ce^{3+} couple [2]. Such a property referred to as oxygen storage capacity (OSC) plays an important role in maintaining the activity of TWCs in a large range of air/fuel ratio. Moreover, the presence of ceria promotes noble metal dispersion [3]. In addition, reductive pre-treatments on ceria supported noble metals can induce considerable changes in the reactivity and adsorptive properties through the so called *strong metal–support interaction* (SMSI) [4]. The possibility that some kind of SMSI can affect the activity of Pt–CeO_2 based catalysts was considered by different authors [5–7].

Recently, we have investigated by several techniques the structural modification and the metal–support interaction established in Pt/ceria–zirconia systems [8–11]. The role of Pt/ceria–zirconia interface in providing oxygen active species during anaerobic CO oxidation tests was highlighted by transient reactivity tests coupled with DRIFT experiments [8], while the

* Corresponding author. Tel.: +39 091 6809371; fax: +39 091 6809399.
E-mail address: liotta@pa.ismn.cnr.it (L.F. Liotta).

0926-3373/$ – see front matter © 2009 Elsevier B.V. All rights reserved.
doi:10.1016/j.apcatb.2009.04.007

structural modifications occurring were investigated by XRD experiments in situ [9]. On the same Pt/ceria–zirconia system SAXS experiments evidenced a noticeable redispersion of Pt upon a reduction treatment at 1050 °C suggesting the occurrence of a Pt–ceria alloying phenomena [10]. In a successive study, the formation of a Pt–Ce alloy confirmed by EXAFS analysis was stated as the reason of the peculiar reactivity properties of redox aged Pt/ceria–zirconia catalysts [11]. Moreover, a positive effect of successive redox cycles on the ceria–zirconia structural reorganization towards the nominal composition of $Ce_{0.6}Zr_{0.4}O_2$ and on the increased OSC values was demonstrated [12].

On the basis of our background, we have prepared a cordierite monolithic $Pt/Ce_{0.6}Zr_{0.4}O_2$ catalyst in order to produce a more realistic TWC system.

By the 1970s over 30 years of catalyst technology, development has been devoted to the automotive exhausts catalysts in order to enhance the catalytic performances and the high-temperature durability. The general trend has been an increase of complex catalyst formulations in responses to increasingly stringent emission standards. However, given the high temperatures and wide-ranging exhausts compositions that TWCs encounter over the life of the vehicle, a multitude of solid-state reactions between the various components of the catalysts can take place along with poisoning and sintering of active noble metals. Therefore, quantitative information is needed about how catalyst aging affects the performances of TWCs.

Recent studies have been devoted to the aging effects on the properties and catalytic performances of commercial TWCs [13–16]. The growth of fibrous materials, such as aluminate whiskers and nanotubes has been observed in aged automotive Pd- and Pt/Rh-based three-way catalysts [13]. Moreover, the effect of accelerate aging on the microstructure of Pt–Rh three-way catalysts has evidenced that precious metals inter-diffuse between the washcoat layers and alloy during aging, while the loss of Pb, Zn, Ca and Ni elements to the environment has been proven [14,15]. The effect of catalyst aging on the activity and selectivity of TWCs has been also addressed. Generally, the TWC activity decreases by catalyst ageing, however, it was found that the NO reduction was less affected compared to the oxidation reactions [16]. Furthermore, it was demonstrated that Pd particle size strongly affects the oxygen storage capacity of Pd/CeO_2 catalysts [17].

On these bases, the detailed characterization of the structural and catalytic modifications occurring in aged TWC systems appears fundamental for designing new better performing catalytic devices.

The present paper focuses on the synthesis of a Pt/ceria–zirconia catalyst over alumina-washcoated cordierite and on the structural modifications occurring upon redox cycles. An accurate XRD analysis and Rietveld refinement of the structural data were performed. Reduction properties of structured Pt/ceria–zirconia/alumina catalyst and of the corresponding monolithic ceria–zirconia were studied by TPR experiments. The influence of redox cycles on the CO oxidation activity at low temperature was investigated. The effect of the catalyst redox aging on the selective catalytic reduction (SCR) of NO by C_3H_6, in lean conditions, was also examined.

Structural and morphological properties, washcoat homogeneity and composition of a redox cycled Pt/ceria–zirconia catalyst were checked by transmission electron microscopy (TEM) and scanning electron microscopy/energy-dispersive X-ray (SEM/EDX) analyses.

2. Experimental

2.1. Catalyst preparation

The ceria–zirconia mixed oxide with nominal composition $Ce_{0.6}Zr_{0.4}O_2$ was synthesised by sol–gel method and calcined at 650 °C for 8 h, according to the procedure described elsewhere [12]. The so prepared powder sample, labelled as pCeZr fresh, showed specific surface area of 45 m^2/g, as determined by BET method.

Commercial cordierite (Corning) with a cell density of 400 cpsi was cut to obtain samples with 25 channels on the cross-section and different lengths up to 40 mm. In order to obtain a washcoat layer of ceria–zirconia onto the cordierite surface, highly dispersed pseudobohemite alumina powder (Disperal, Sasol) was used as a binder [18]. The monoliths were dipped in a slurry composed of diluted nitric acid solution (1.4 wt%) and appropriate amounts of finely grounded ceria–zirconia and pseudobohemite powders in order to obtain a final washcoat composition of ceria–zirconia (80 wt%)-γ-Al_2O_3 (20 wt%). Several dips were needed to obtain the desired amount of washcoat loading (25% of the total weight). In each cycle the excess slurry was removed by blowing air through the channels and then the samples were dried at 120 °C for 1 h and calcined at 550 °C for 3 h for binder decomposition and γ-Al_2O_3 stabilization.

The prepared monolithic alumina supported ceria–zirconia sample (mCeZrAl fresh) was impregnated with platinum (1 wt% with respect to the ceria–zirconia weight content) by using a solution of $Pt(acac)_2$ in toluene at 70 °C, then calcined at 400 °C for 5 h. The resulting catalyst, labelled as mPtCeZrAl fresh, showed a specific surface area of 15 m^2/g (the value refers to the total weight of the monolith).

Reference powder ceria–zirconia–alumina samples were also prepared after drying and calcination at 550 °C for 3 h of the same slurry used for washcoating monolith. Pt(1 wt%) over ceria–zirconia–alumina powder was deposited by impregnation (pPtCeZrAl fresh).

2.2. Catalyst characterization

Characterizations of the catalysts were performed directly on the monoliths opportunely sectioned, unless differently specified. Moreover, for reproducibility check, some analyses were also performed over the powder catalyst references.

The X-ray diffraction (XRD) analyses were performed with a Philips (PW1820) vertical goniometer connected to a highly stabilized generator (Philips PW 1830), using nickel-filtered Cu-Kα radiation (λ = 1.5418 Å). The spectra were collected using a step size of 0.05° and a counting time of 20 s per angular abscissa. The assignment of the crystalline phases was based on the JPDS powder diffraction file cards [19]. The particle sizes of different phases were calculated from the line broadening of the most intense reflections using the Scherrer equation [20].

The XRD data were analysed according to the Rietveld method using the GSAS package program [21,22]. The goodness of fit and profile agreement were checked by low values (<0.05) of R_p and R_{wp} indexes [23]. The fitting procedure allowed to refine lattice constants, thermal disorder, atomic positions and occupancy factors. The stoichiometry of Ce and Zr in the phases and the relative weight fraction were also determined by Rietveld refinement, as previously reported [12].

Specific surface area was evaluated by BET method using a Carlo Erba 1900 Sorptomatic apparatus.

Temperature programmed reduction (TPR) was carried out with a Micromeritics Autochem 2910 apparatus equipped with a thermal conductivity detector. In order to minimize the contribution from adsorbed species to the TPR, all the samples opportunely sectioned (~350 mg of monolith or 100 mg of powder catalyst) were pre-treated with 5%O_2/He at 500 °C for 30 min and cooled down under He to room temperature, then the reducing mixture 5%H_2/Ar (50 ml/min) was left flowing while heating to 1050 °C at a rate of 10 ° C/min. Three consecutive reduction–oxidation cycles

Table 1
Structural parameters by Rietveld refinement of ceria–zirconia and Pt/ceria–zirconia samples, as prepared or after three redox cycles.

Sample	Phase composition and relative weight fraction (wt%)	Lattice constant (Å)	d_{CeZr} (nm)
pCeZr fresh	$Ce_{0.75}Zr_{0.25}O_2$ (65)	*a*, *b*, *c* = 5.351	8
	$Ce_{0.42}Zr_{0.58}O_2$ (35)	*a*, *b* = 3.695; *c* = 5.302	9
mCeZrAl redox	$Ce_{0.61}Zr_{0.39}O_2$ (15)	*a*, *b*, *c* = 5.311	35
	$Ce_{0.48}Zr_{0.52}O_2$ (65)	*a*, *b* = 3.732; *c* = 5.305	35
	$CeAlO_3$ (20)	*a*, *b* = 3.767; *c* = 3.797	–
mPtCeZrAl redox	$Ce_{0.62}Zr_{0.38}O_2$ (100)	*a*, *b*, *c* = 5.311	36

were performed calcining with 5%O_2/He at 500 °C for 30 min the above reduced samples, after cooling to r.t. in He. The resulting redox cycled catalysts were labelled as p or m(Pt)CeZrAl redox, according to the status, powder or monolith.

TEM analyses were performed on the powder catalysts by using a JEOL 2010 LaB6 instrument working at 200 kV equipped with an Oxford Instrument Link ISIS EDX system for electron probe microanalysis. Suspensions of the samples in ethanol were dropped on carbon-coated grid and after evaporating the solvent electron micrographs of the particles were taken.

SEM images and EDX analyses were recorded using a Philips XL30 ESEM microscope.

2.3. Catalytic tests

CO oxidation tests were performed by using a quartz tube in a furnace electrically heated. The external and central channels of the monolith were blocked at both ends with ceramic wool. A K-type thermocouple inserted in the central channel was used to measure the monolith temperature. The reagent gas mixture composition was 1% CO + 1% O_2 in He. The gas hourly space velocity (GHSV) was fixed at 10,000 h^{-1} by changing the gas flow rate opportunely depending on the monolith volume.

Before the tests, the samples were pretreated "in situ" under flowing 5%O_2/He at 500 °C for 30 min and cooled down under He to room temperature. Activities were measured by increasing the temperature from 25 to 250 °C, by steps of 25 °C (holding time 30 min at each temperature). In the case of Pt-free Ce–Zr catalysts, due to the poor activity, the temperature was increased up to 800 °C, by steps of 50 °C, in order to obtain nearly full CO conversion. The CO and CO_2 effluent gases were monitored by IR analyser (ABB Uras 14) and by on line mass quadrupole spectrometer (Thermostar™, Balzers).

The selective catalytic reduction (SCR) of NO by propylene was investigated over the sample mPtCeZrAl redox, by feeding a mixture containing 0.2% NO, 0.2% C_3H_6, 2%O_2 in He. The GHSV was fixed at 10,000 h^{-1} and activities were measured by increasing the temperature from 150 to 400 °C, by steps of 25 °C (holding time 30 min at each temperature). Before test, the catalyst was reduced "in situ" flowing 5%H_2/Ar at 350 °C for 1 h, then was cooled to 100 °C under He. Reactants and products concentrations were monitored by IR/UV analysers (ABB Uras 14, Limas 11) and by on line mass quadrupole spectrometer (Thermostar™, Balzers).

3. Results and discussion

3.1. XRD characterization

The XRD characterization of the pCeZr fresh showed the presence of broad shaped peaks suggesting the presence of highly dispersed crystallites and the co-existence of at least two solid solutions, according to previously reported data [12]. Accordingly, crystallite particle size of ~8 nm were calculated and two ceria–zirconia solutions, a ceria-rich cubic phase with composition $Ce_{0.75}Zr_{0.25}O_2$ and a tetragonal zirconia-rich phase with composition $Ce_{0.42}Zr_{0.58}O_2$, were evidenced by Rietveld refinement of the structural data (see Table 1 for *a*, *b*, *c* lattice parameters). Being the c/a lattice ratio >1, the tetragonal phase was identified as *t*′ [12]. Moreover, the presence of some amorphous ceria impurity cannot be discounted.

Upon deposition of the ceria–zirconia powder over the cordierite substrate and successive calcinations at 550 °C no structural modifications take place. Moreover no Pt particles of XRD detectable size are obtained after platinum impregnation.

A structural reorganization of the ceria–zirconia along with a large sintering of crystallites (*d* = 36 nm, Table 1) occurs when three successive redox cycles were performed over the Pt/ceria–zirconia monolith. In Fig. 1a the XRD pattern recorded over the reference pPtCeZrAl redox is displayed. For comparison, the pattern of the mPtCeZrAl redox cycled is shown in Fig. 1b. As concerns ceria–zirconia features, sintering of crystallites is pointed by the sharpness of the peaks. Furthermore, a structural reorganization of the two solid solutions into a single cubic one with composition $Ce_{0.6}Zr_{0.4}O_2$ takes place, as it is evident from the

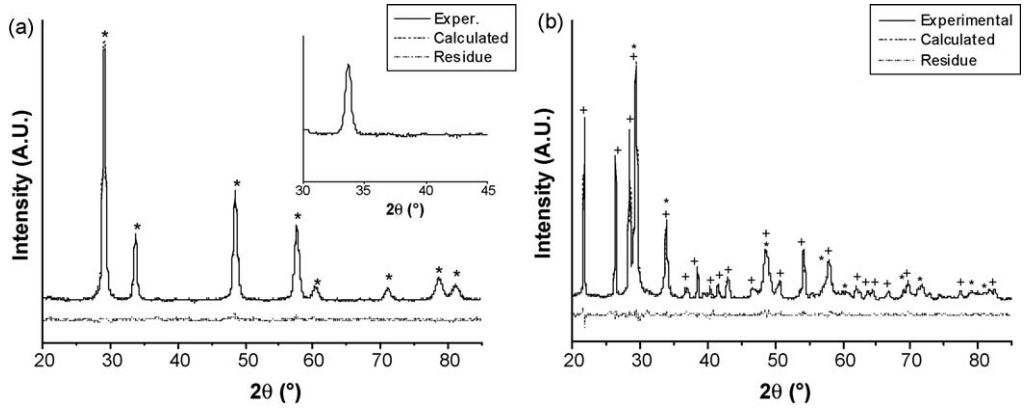

Fig. 1. Experimental and calculated XRD patterns of: (a) pPtCeZrAl redox; (b) mPtCeZrAl redox (the symbols refer to the following phases: $^*Ce_xZr_{(1-x)}O_2$, $^+$cordierite).

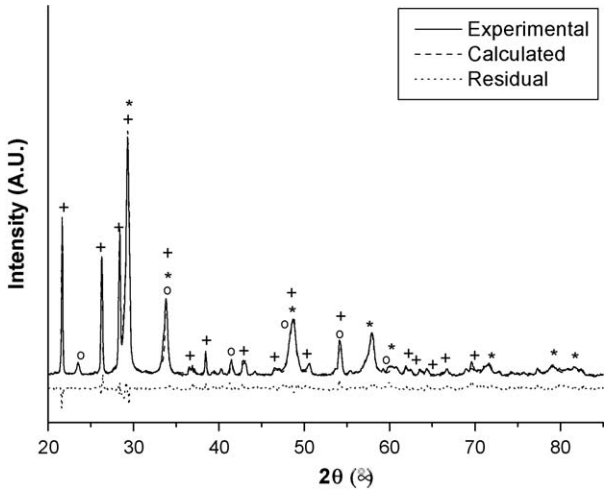

Fig. 2. Experimental and calculated XRD patterns of mCeZrAl redox (the symbols refer to the following phases: $^{*}Ce_xZr_{(1-x)}O_2$, $^{\circ}CeAlO_3$, $^{+}$cordierite).

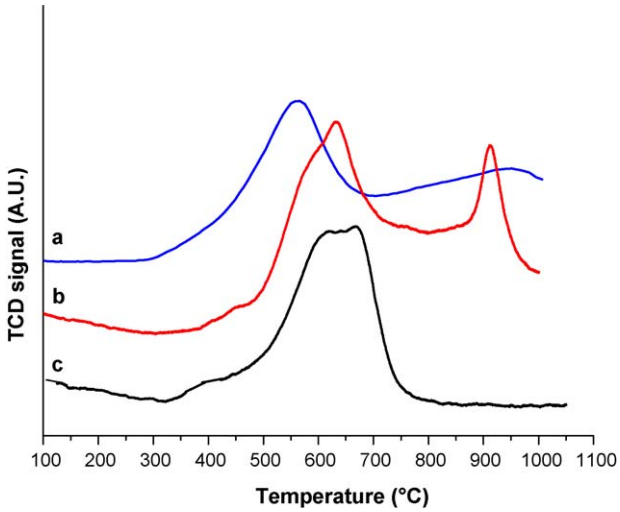

Fig. 3. First, second and third TPR profiles (a, b, c) of mCeZrAl.

symmetric shape of the peaks and as confirmed by Rietveld analysis and calculated lattice constants (Table 1). Looking at the angular range 38–42° 2θ, no features attributable to platinum phases (PtO_x nor Pt^0) of detectable size are visible (see inset of Fig. 1a).

From the data so far reported, important information concerning the remarkable stability of the redox cycled Pt catalyst arises. The occurrence of a SMSI interaction between Pt–Ce, probably a Pt–Ce alloy as previously demonstrated [10,11], well accounts for maintaining Pt crystallites highly dispersed even after three consecutive redox treatments up to 1050 °C in reducing atmosphere. On the contrary, in oxidative atmosphere no metal–support interaction is observed and sintering of Pt aggregates occurs when the catalyst was calcined to 1050 °C [10].

However, the major novelty concerning the effect of platinum in the stabilization of ceria–zirconia solid solution, in presence of alumina, comes from the comparison with the XRD pattern recorded on ceria–zirconia metal free upon three redox cycles. The presence of a sharp peak attributed to the $CeAlO_3$ phase is well evident in the XRD pattern recorded over mCeZrAl redox (Fig. 2) and it was also confirmed over the powder sample redox aged. It is worth to notice that platinum is effective towards the stabilization of ceria–zirconia in the presence of alumina. Actually, in the XRD patterns of the redox-cycled Pt/ceria–zirconia/alumina samples only the peaks of ceria–zirconia and cordierite (Fig. 1a and b) can be recognized. On the contrary, in the metal-free sample mCeZrAl redox (Fig. 2) the presence of a $CeAlO_3$ phase is well evident. Such phase is formed during the reduction treatment as a consequence of the solid-state reaction between Ce^{3+} and the alumina phase present in the washcoat. As a consequence of cerium depletion, the zirconia richer solid solution becomes the main phase (65 wt%), followed by $CeAlO_3$ (20 wt%) and $Ce_{0.61}Zr_{0.39}O_2$ (15 wt%) (see Table 1). Alike mPtCeZrAl, sintering of ceria–zirconia crystallites (d = 35 nm, Table 1) occurs upon redox aging. At the same time, a decrease of the specific surface area values to 2.1 and 0.8 m^2/g for mPtCeZrAl and mCeZrAl redox, respectively, takes place.

3.2. TPR characterization

In Fig. 3 three consecutive TPR profiles recorded over the ceria–zirconia monolithic sample are shown. The first curve (Fig. 3, curve a) shows a main reduction peak, with a hydrogen consumption of 1.2 mmol H_2/g_{CeZr}, centred at 560 °C attributed to the reduction of Ce^{4+} present in Ce–Zr solid solutions. It is known that in Ce–Zr solid solutions the reduction of ceria occurs concurrently at the surface and in the bulk [24,25]. Attribution of the reduction feature at ~500 °C to the surface layer reduction of some ceria impurity cannot be excluded. Indeed, at variance with ceria–zirconia, the reduction process of pure ceria at 400–500 °C is strictly surface-related while at high temperature, 800–900 °C, the reduction of ceria bulk takes place [26–29]. On this basis, the peak at 950 °C (Fig. 3, trace a) has been ascribed to the reduction of ceria bulk. Moreover, due to the presence of the alumina washcoat in the monolith, formation of bulk $CeAlO_3$ phase as a consequence of the reduction of Ce^{4+} may occur [30]. TPR profiles recorded successively, as second and third runs (Fig. 3, curves b,c), differ from the first curve for position and shape of the peaks. In the second curve, the peak at low temperature (0.98 mmol H_2/g_{CeZr}) shifts to higher values, at 630 °C; while a sharp peak, centred at 920 °C, is observed at high temperature. Interestingly, when a third cycle is run, only a single reduction feature (0.92 mmol H_2/g_{CeZr}) centred at about 650 °C is detected. The observed differences seem to confirm that redox cycles induce a modification of ceria–zirconia composition likely due to a reorganization of the solid-solution and/or to $CeAlO_3$ formation [12,29,30]. Indeed, in the second TPR, the shift of the low-temperature reduction peak to higher values, to ~630 °C, suggests the presence of a Zr-enriched solid solution as the main phase [28], in agreement with Rietveld results (Table 1). Moreover, the increased peak at 920 °C confirms that in reducing conditions formation of $CeAlO_3$ by diffusion of Ce^{3+} into the alumina washcoat takes place [30]. It is worth to notice that the hydrogen consumption (0.35 mmol H_2/g_{CeZr}) well accounts for the quantitative reduction of Ce^{4+} to Ce^{3+} corresponding to a $CeAlO_3$ content of 20 wt% (see Table 1). Reoxidation of Ce^{3+}, if present as $CeAlO_3$, is known to occur slowly and upon long oxidation treatments above 1000 °C [30–32]. Consequently, it is likely that, once $CeAlO_3$ is formed during the second TPR, a further oxidation treatment at 500 °C does not affect this phase, which remains stable. The almost constant hydrogen consumption (around 0.92 mmol H_2/g_{CeZr}) along with the observation that no further reduction at around 900 °C occurs during the third TPR confirms such idea and, at the same time, suggests that no more $CeAlO_3$ formation occurs during the third TPR. Redox cycles performed over different portions of the CeZrAl washcoated monolith as well as over the reference pCeZrAl were well reproducible confirming the trend of Fig. 3.

When three successive redox cycles are performed over mPtCeZrAl, the reduction of the ceria–zirconia oxide is favoured by the presence of Pt which increases the lattice oxygen mobility (Fig. 4 curves a, b, c). Accordingly, the first TPR profile (curve a) contains as major contribution a peak, at low temperature, centred

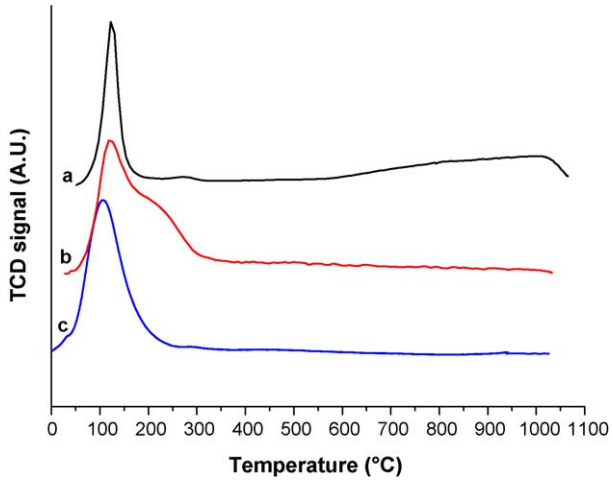

Fig. 4. First, second and third TPR profiles (a, b, c) of mPtCeZrAl.

at 125 °C. This peak with a hydrogen uptake of 0.73 mmol/g_{PtCeZr} contains contribution from the reduction of highly dispersed α-PtO_2 species along with from the reduction of the Ce–Zr support [29]. Moreover, similarly to what observed in the first TPR of Ce–Zr, a peak at around 1000 °C is visible. This high temperature reduction feature disappears when the second and third TPR are performed (Fig. 4 curves b, c). In the second TPR reduction occurs between 120–200 °C, while in the third TPR a single peak at 100 °C is observed. The asymmetric shape of the second profile (Fig. 4, trace b) suggests that during the second reduction a structural reorganization of the ceria–zirconia solid solution, by incorporating ceria impurity, takes place. Whereas, the presence in the third TPR (Fig. 4, trace c) of a single reduction feature is consistent with the presence of a crystallographic pure Ce–Zr phase [25] and confirms previous data claiming the presence of a single peak below 200 °C in the reduction profile of a redox cycled Pt/$Ce_{0.5}Zr_{0.5}O_2$ catalyst [29]. The possibility that in mPtCeZrAl residual ceria is incorporated into the Ce–Zr lattice is also supported by the increased hydrogen consumption (0.85 mmol/g_{PtCeZr}) in the second TPR. Such value remains constant in the further third reduction and accounts for the reduction of both PtO_2 species and Ce–Zr.

On the basis of XRD and TPR data so far reported, a key role played by Pt towards the stabilization of ceria–zirconia, in presence of alumina, emerges. The reason for stabilization may be related to the hydrogen activation by metallic Pt, in analogy with other noble metals, with subsequent spillover on the Ce–Zr support and consequent reorganization of the structural composition and promotion of the reduction at lower temperature. Moreover, the occurrence of a SMSI interaction between Pt–Ce, may reasonably stabilize ceria against diffusion into the alumina bulk.

3.3. TEM and SEM/EDX investigations

Fig. 5(a, b) shows two transmission electron micrographs of the catalyst pPtCeZrAl redox, at different magnification. Due to the low contrast with the support, the Pt and Ce–Zr particles cannot easily be distinguished to each other. However, a careful analysis by EDX allows identifying the two phases, as shown in Fig. 5, where Ce–Zr crystallites with diameter between 10 and 35 nm were detected, while Pt particle sizes as small as 2–3 nm are present. It is worth noting that platinum was always found as Pt–Ce–Zr small aggregates, not as isolated Pt particles, confirming that an interaction Pt–Ce takes place. On the contrary, well dispersed Ce–Zr–Pt particles as well as big Ce–Zr clusters are detected. The Pt particle sizes calculated by TEM characterization are well consistent with XRD dimensions by Scherrer equation (Table 1) and are in quite good agreement with our previous results by small-angle X-ray scattering and EXAFS [10,11].

In order to check the quality of the coatings of the structured Pt/ceria–zirconia catalyst, after performing three redox cycles, SEM investigations were carried out over the washcoated monoliths opportunely sectioned. Upon SEM inspection of the longitudinal section, the channels appear uniformly covered by a smooth active layer (Fig. 6a). EDX microanalyses evidence the presence of uniform superficial Pt coverage all along the length of the channel, but for a slight enrichment in a thin outer zone of the samples. The layer thickness is quite uniform with a minimum value of about 10 μm on the walls, which rises up to 80–100 μm in the corners, giving the classical rounded shape to the originally square channels (Fig. 6b). This layer is firmly anchored to cordierite walls: average weight loss after 20 min in ultrasonic bath is limited to 0.7% of the washcoat weight. At higher magnification (Fig. 6c, d) the washcoat appears to be made of small grains with size ≤1 μm, joined together within an alumina matrix deriving from binder decomposition and partially sintered due to high temperature treatment (1050 °C in H_2 5%/Ar). Moreover, EDX maps recorded in several different sections of the washcoat (an example is reported in Fig. 7 for a 40 μm depth) clearly show that a very homogeneous distribution of each element is obtained in the whole catalytic

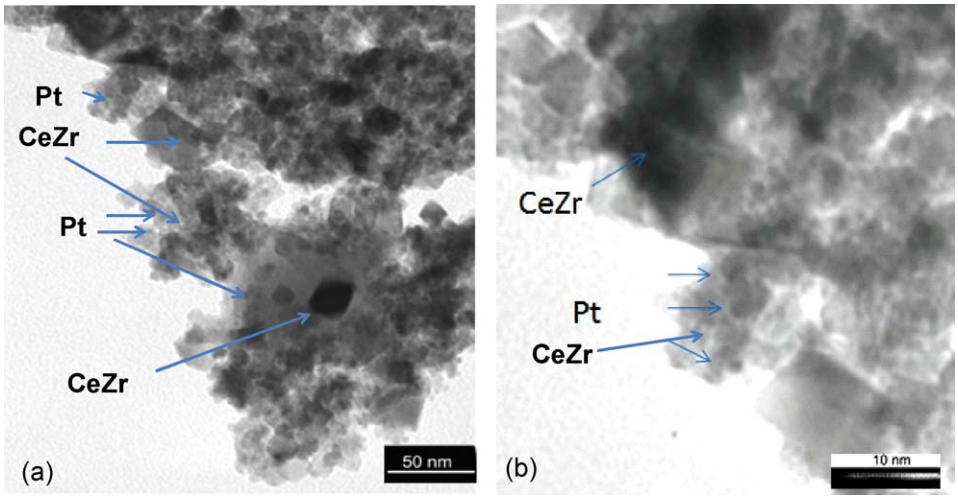

Fig. 5. TEM images (a, b) of pPtCeZrAl redox at two different magnifications.

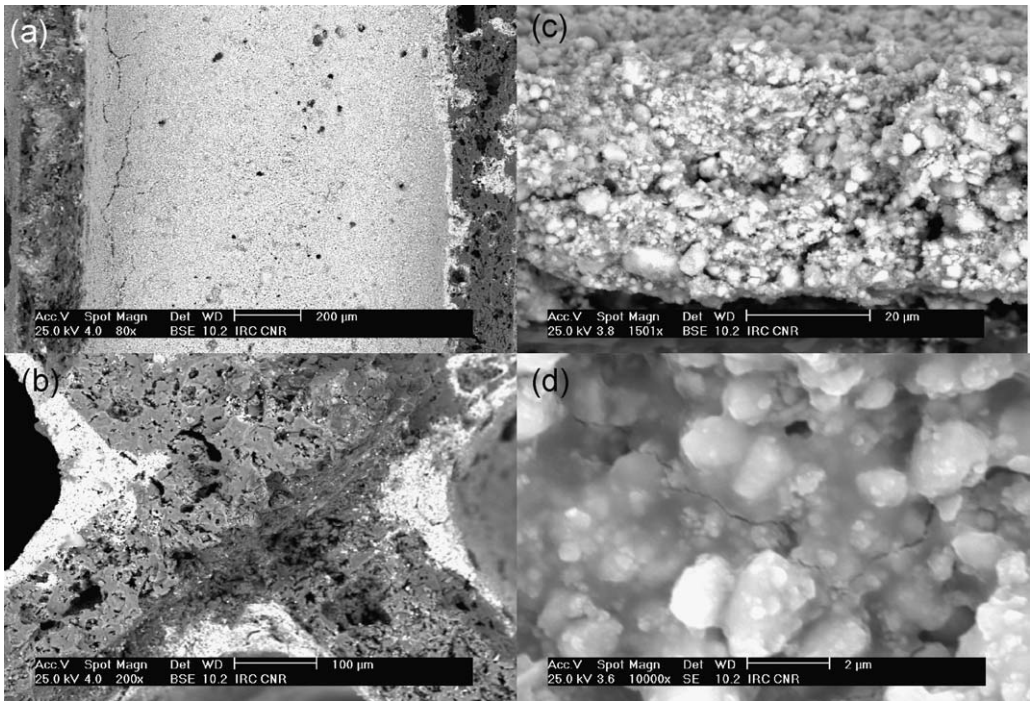

Fig. 6. SEM micrographs of mPtCeZrAl redox: (a) longitudinal section of the channel; (b) details of the corners; (c, d) details of the longitudinal view of the channels.

layer. In particular the penetration depth of the precious metal precursor is very satisfactory. Fig. 8 shows that Ce–Zr and Pt atomic contents are in line with the nominal values (Ce/Ce + Zr = 60 and Pt = 0.8 at%) and present a rather constant profile as a function of the distance from the external surface of the washcoat.

In conclusion, it results that washcoat preparation strategy, previously reported to provide an elevated attrition resistance and high permeability in the case of perovskites supported on La stabilized γ-Al_2O_3 washcoated monoliths [18], led to an homogeneous and uniform coverage of channels also starting with ceria–zirconia powders. Moreover, the active components of Pt/ceria–zirconia catalyst remain quite uniformly distributed over the alumina washcoated monolith after three successive redox cycles up to 1050 °C.

3.4. Activity tests

The catalytic performances of mPt/CeZrAl, as prepared and after three redox cycles were investigated in the CO oxidation and compared with the analogous metal-free mCeZrAl samples (Fig. 9). In Table 2 the temperature of 50% and 100% of CO conversion are listed. The highest activity is shown by the Pt catalyst redox cycled, which performs better than the untreated sample and compares well with literature results [33,34]. The activity of ceria–zirconia monolith is significantly lower and further decreases after three redox cycles. Catalytic data are completely in agreement with structural and morphological results, confirming the enhancement of the catalytic activity of the structured Pt catalyst upon redox cycles. On the contrary,

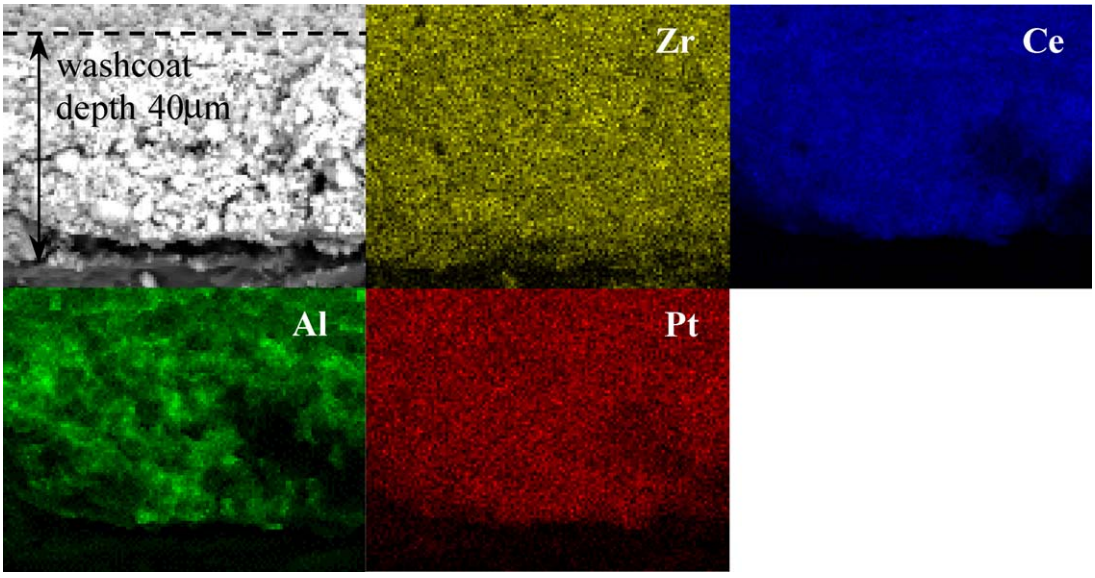

Fig. 7. EDX maps recorded in the channels section of mPtCeZrAl redox for a 40 µm depth.

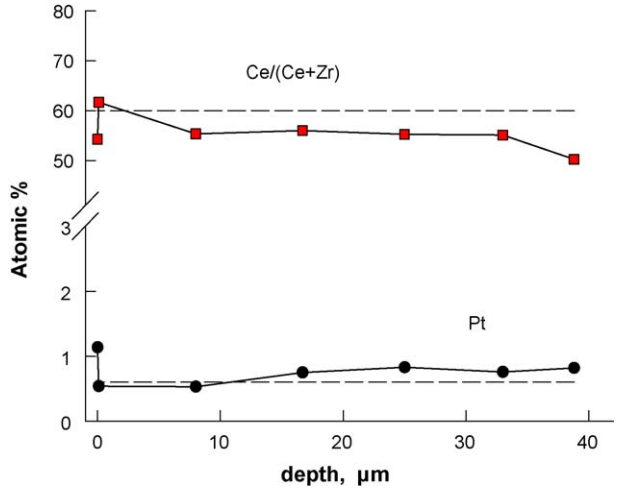

Fig. 8. Pt, Ce, Zr elements composition for a washcoat depth of 40 μm, as derived by EDX analysis of mPtCeZrAl redox.

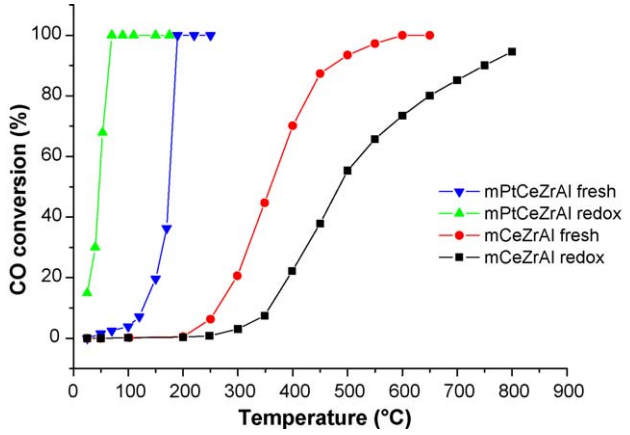

Fig. 9. CO conversion curves as a function of the temperature for the different monolithic catalysts. Feed composition: 1% CO, 1% O_2 in He.

redox cycles performed over the ceria–zirconia monolith are detrimental due to the $CeAlO_3$ formation.

Moreover, the TPR data indicate a good correlation between reduction properties and oxidation activity. The high oxygen mobility of a $Ce_{0.6}Zr_{0.4}O_2$ solid solution in good contact with highly dispersed Pt clusters appears a key factor for the enhanced oxidation activity.

Typical results of the SCR of NO by C_3H_6 in excess of oxygen over the catalyst mPtCeZrAl redox are presented in Fig. 10 where the conversions of NO (X_{NO}) and C_3H_6 ($X_{C_3H_6}$) as well as the yield of N_2 (Y_{N_2}) and N_2O (Y_{N_2O}) are plotted as function of the reaction temperature. The C_3H_6 conversion to CO_2 increases sharply with increasing the reaction temperature above 250 °C and reaches completion at 290 °C. A parallel increase of the NO conversion to N_2 and N_2O is observed with a maximum value of 55% of NO conversion at 290 °C. The selectivity towards N_2 at this temperature was of 50% and then slightly decreases by further increasing the temperature.

Table 2
Temperature in correspondence of the 50% and 100% conversion of CO.

Catalyst	$T_{50\%}$ (°C)	$T_{100\%}$ (°C)
mPtCeZrAl fresh	175	200
mPtCeZrAl redox	43	69
mCeZrAl fresh	360	600
mCeZrAl redox	485	>800

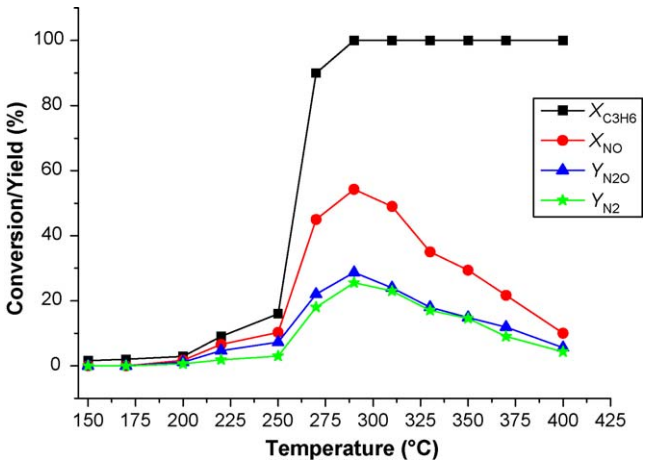

Fig. 10. Conversions (%) of NO (X_{NO}) and propylene ($X_{C_3H_6}$) and yields (%) of N_2 (Y_{N_2}) and N_2O (Y_{N_2O}) for the catalyst mPtCeZrAl redox as functions of reaction temperature. Feed composition: 0.2% NO, 0.2% C_3H_6, 2% O_2 in He.

Under the present experimental conditions formation of NO_2 was negligible up to 400 °C. The present data are in agreement with the well-known performances of platinum group metals supported on ceria–zirconia for SCR of NO to N_2 by C_3H_6 [10,35].

4. Conclusion

From this study, the following important results can be summarized:

The achievement of a well performing and highly stable alumina-supported Pt/ceria–zirconia monolith strongly depends on the nature of pre-treatments.

Pt affects positively the reorganization of ceria–zirconia solid solution also in presence of alumina preventing $CeAlO_3$ formation, which is detrimental for the catalytic activity. The stabilizing effect of platinum is interpreted in terms of Pt–Ce SMSI which hinders Ce^{3+} diffusion. TEM characterization confirms that Pt is present as highly dispersed particles (2–3 nm) strongly interacting with the ceria-based support.

These findings are fundamental for obtaining a durable Pt/ceria-zirconia/alumina catalyst well performing, at low-temperature, in CO oxidation as well as in the SCR of NO to N_2 by C_3H_6.

The structural, morphological and reduction properties of the samples well account for the observed catalytic behaviour.

References

[1] R.M. Heck, R.J. Farrauto, S.T. Gulati, Catalytic Air Pollution Control, second ed., J. Wiley & Sons, Inc. Publication, New York, 2002 (Chapter 6).
[2] A. Trovarelli, Catalysis by ceria and related materials, in: G.J. Hutchings (Ed.), Catalytic Science Series, vol. 2, Imperial College Press, London, 2002.
[3] J. Kaspar, P. Fornasiero, M. Graziani, Catal. Today 50 (1999) 285.
[4] S. Bernal, J.J. Calvino, M.A. Cauqui, J.M. Gatica, C. Larese, J.A. Pérez Omil, J.M. Pintado, Catal. Today 50 (1999) 175.
[5] S.E. Golunski, H.A. Hatcher, R.R. Rajaram, T.J. Truex, Appl. Catal. B 5 (1995) 367.
[6] A. Holmgren, B. Andersson, J. Catal. 178 (1998) 14.
[7] C. Bozo, N. Guilhaume, J.-M. Herrmann, J. Catal. 203 (2001) 393.
[8] G.E. Arena, G. Centi, G. Deganello, L.F. Liotta, A. Macaluso, G. Pantaleo, Top. Catal. 30/31 (2004) 397.
[9] A. Martorana, G. Deganello, A. Longo, A. Prestianni, L. Liotta, A. Macaluso, G. Pantaleo, A. Balerna, S. Mobilio, J. Solid State Chem. 177 (2004) 1268.
[10] L.F. Liotta, A. Longo, A. Macaluso, G. Pantaleo, A.M. Venezia, G. Deganello, Appl. Catal. B 48 (2004) 133.
[11] G. Deganello, F. Giannici, A. Martorana, G. Pantaleo, A. Prestianni, A. Balerna, L.F. Liotta, A. Longo, J. Phys. Chem. B 110 (2006) 8731.
[12] L.F. Liotta, A. Macaluso, A. Longo, G. Pantaleo, A. Martorana, G. Deganello, Appl. Catal. A 240 (2003) 295.
[13] J. Hangas, Catal. Lett. 86 (2003) 267.

[14] J. Hangas, A.E. Chen, Catal. Lett. 108 (2006) 103.
[15] R. Fernández-Ruiz, F.C. Galisteo, C. Larese, M.L. Granados, R. Mariscal, J.L.G. Fierro, Analyst 131 (2006) 590.
[16] J.H. Baik, H.J. Kwon, Y.T. Kwon, I.-S. Nam, S.H. Oh, Top. Catal. 42/43 (2007) 337.
[17] S.Y. Christou, A.M. Efstathiou, Top. Catal. 42/43 (2007) 351.
[18] S. Cimino, L. Lisi, R. Pirone, G. Russo, M. Turco, Catal. Today 59 (2000) 19.
[19] JCPDS Powder Diffraction File, Int. Centre for Diffraction Data, Swarthmore.
[20] H.P. Klug, L.E. Alexander, X-ray Diffraction Procedures for Polycrystalline and Amorphous Materials, Wiley, New York, 1954.
[21] H.M. Rietveld, J. Appl. Crystallogr. 2 (1969) 65.
[22] A. Larson, R.B. Von Dreele, Report LAUR 86-748, Los Alamos Laboratory, Los Alamos, NM, 1988.
[23] R.J. Hill, I.C. Madsen, J. Appl. Crystallogr. 19 (1986) 10.
[24] P. Fornasiero, G. Balducci, R. Di Monte, J. Kaspar, V. Sergo, G. Gubitosa, A. Ferrero, M. Graziani, J. Catal. 164 (1996) 173.
[25] G. Balducci, J. Kaspar, P. Fornasieo, M. Graziani, M.S. Islam, J. Phys. Chem. B 102 (1998) 557.
[26] P. Vidmar, P. Fornasiero, J. Kaspar, M. Graziani, J. Catal. 171 (1997) 160.
[27] F. Fally, V. Perrichon, H. Vidal, J. Kaspar, G. Blanco, J.M. Pintado, S. Bernal, G. Colon, M. Daturi, J.C. Lavalley, Catal. Today 59 (2000) 373.
[28] H. Vidal, J. Kaspar, M. Pijolat, G. Colon, S. Bernal, A. Cordon, V. Perrichon, F. Fally, Appl. Catal. B 30 (2001) 75.
[29] P. Fornasiero, J. Kaspar, V. Sergo, M. Graziani, J. Catal. 182 (1999) 56.
[30] A. Piras, A. Trovarelli, G. Dolcetti, Appl. Catal. B 28 (2000) L77.
[31] K. Bak, L. Hilaire, Appl. Surf. Sci. 70/71 (1993) 191.
[32] V. Pitchon, J.F. Zins, L. Hilaire, G. Maire, React. Kinet. Catal. Lett. 59 (1996) 203.
[33] J. Fan, X. Wu, R. Ran, D. Weng, Appl. Surf. Sci. 245 (2005) 162.
[34] J.L. Ayastuy, M.P. Gonzalez-Marcos, A. Gil-Rodriguez, J.R. Gonzalez-Velasco, M.A. Gutierrez-Ortiz, Catal. Today 116 (2006) 391.
[35] C. Thomas, O. Gorce, F. Villain, G. Djéga-Mariadassou, J. Mol. Catal. A 249 (2006) 71.